Manuscript for Annual Meeting Compendium of Papers

Quantification of Lateral Forces in Concrete Crosstie Fastening Systems

TRB 15-1534

Transportation Research Board 94th Annual Meeting

Submitted: 15 November 2014

Brent A. Williams[1,2], Marcus S. Dersch[2], J. Riley Edwards[2], and Christopher P. L. Barkan[2]

[2]*Rail Transportation and Engineering Center – RailTEC*
Department of Civil and Environmental Engineering
University of Illinois at Urbana-Champaign
205 N. Mathews Ave., Urbana, IL 61801

3,800 Words, 8 Figures = 5,800 Total Word Count

Brent A. Williams	Marcus S. Dersch	J. Riley Edwards
(603) 562-5515	(217) 333-6232	(217) 244-7417
bwillms3@illinois.edu	mdersch2@illinois.edu	jedward2@illinois.edu

Christopher P. L. Barkan
(217) 244-6338
cbarkan@illinois.edu

[1]Corresponding author

ABSTRACT

Consistent increases in cumulative freight tonnages, combined with the move towards higher-speed intercity passenger rail operation, have placed greater demands on North American railroad infrastructure. Concrete crossties and fastening system components are known to fail at a wide range of life cycle intervals when subjected to demanding loading environments. Such failures can cause track geometry defects, require repetitive maintenance procedures, and present critical engineering challenges. Rail seat deterioration (RSD), the degradation of the concrete material beneath the rail, has been identified through surveys of North American Class I railroads as the most critical engineering challenge of concrete crossties. Shoulder/fastener wear or fatigue was identified through the same survey as the second most critical engineering challenge related to concrete crossties. Lateral forces transferred through the fastening system are thought to be a primary cause of degradation of insulators. The objective of this study is to quantify the demands on the insulator through analysis of the transfer of lateral wheel loads into the fastening system by measuring the magnitude of lateral forces entering the shoulder, a component of the fastening system adjacent to the insulator. The Lateral Load Evaluation Device (LLED) was developed at UIUC to quantify these forces. Data captured by the LLED will assist the rail industry in moving towards the mechanistic design of future fastening systems by quantifying lateral forces in the fastening system under representative loading conditions. Information gained through this study will also lead to a better understanding of the frictional forces at key interfaces in the fastening system. Preliminary results show that the transfer of lateral wheel loads into the fastening system is highly dependent on the magnitude of lateral wheel loads and the frictional characteristics of the fastening system.

Keywords: Lateral force, heavy axle load, friction, concrete crosstie, fastening system design

INTRODUCTION

Concrete crossties and elastic fastening systems are typically installed in demanding loading environments, such as lines with heavy axle load (HAL) freight traffic, high degrees of curvature, steep grades, extreme climates, higher speed rail traffic, or passenger rail traffic which requires strict geometric tolerances. These loading environments may be too demanding for conventional timber crossties, limiting their life cycles and increasing the cost effectiveness of concrete crossties. Although concrete crossties may provide a better option than conventional timber crossties in demanding environments, they are not without their design and performance challenges. Rail seat deterioration (RSD), the degradation of the concrete material beneath the rail, has been identified through surveys of North American Class I railroads as the most critical engineering challenge associated with concrete crossties. Shoulder/fastener wear or fatigue was identified through the same survey as the second most critical engineering challenge for concrete crossties (*1*). Shoulder/fastener wear or fatigue causes excessive rail movement, which expedites the RSD process.

The component located between the rail base and the anchorage point for the elastic clip is commonly referred to as an insulator (Figure 1). The insulator is a critical component given it contacts nearly every other component within the fastening system. However, though the insulator is a critical component, it is also designed to be a sacrificial wear component to prevent the rail or shoulder from wearing. As an insulator wears it can lose the ability to maintain track gauge, attenuate lateral bearing forces to the shoulder, provide electrical isolation, or transmit the design clamping force from the clip to the rail. Furthermore, as an insulator wears, some track geometry defects (e.g. wide gauge) will become more prevalent and excessive rail movement can occur, accelerating failure mechanisms of other fastening system components or the concrete crosstie itself (e.g. rail pad wear and RSD) (*2*, *3*). This presents the engineering challenge of designing an insulator that can withstand the demands at this critical interface while also maintaining the integrity of the entire fastening system.

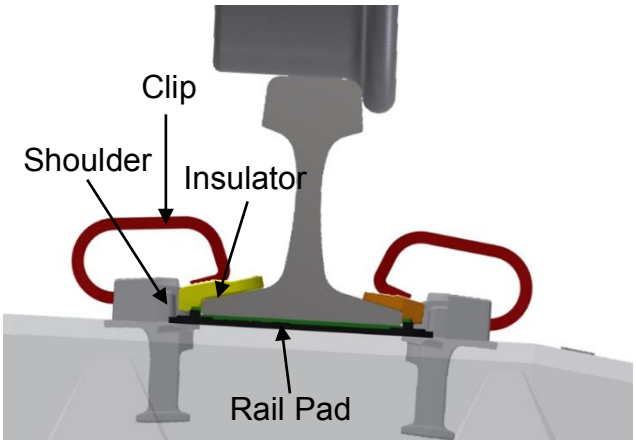

FIGURE 1 Safelok I fastening system component description.

A simplified Failure Mode and Effect Analysis (FMEA) was used to guide our approach to addressing failed insulators. The FMEA was used to define and identify the modes of failure, their causes, and the effects they have on other fastening system components and the system as a whole (*4*). The outcome of the FMEA narrowed our focus to three primary causes of insulator failure: abrasion, fracturing, and crushing. Abrasion occurs when relative motion occurs

between the insulator and the shoulder or rail base. This relative motion, combined with lateral forces acting normal to the insulator, will degrade the insulator. Fracturing of the insulator will occur when lateral forces are applied in a way that causes the component to fracture or crack. Lastly, crushing occurs when the lateral force acting on the insulator exceeds the material property's limits and the insulator deforms plastically. Ultraviolet (UV) light or moisture exposure can also alter material properties and initiate failure (*5*).

By quantifying the lateral forces passing through the insulator and bearing on the shoulder, we gain valuable insight into the demands placed on it, allowing for mechanistic design. Mechanistic design is a process derived from analytical and scientific principles, considering field loading conditions and performance requirements (6). University of Illinois at Urbana-Champaign (UIUC) researchers have designed the Lateral Load Evaluation Device (LLED) to measure the lateral bearing forces acting on the shoulder and aid in the mechanistic design of the fastening system and its components.

MEASUREMENT TECHNOLOGY

UIUC's LLED has two defined points of contact with the shoulder that act as outer supports and two defined points of contact with the insulator that are narrower than the supports. Under load, this specific geometry induces a bending action of the beam. The beam contains four strain gauges which are wired into a full Wheatstone Bridge to measure bending strain under load. Two strain gauges are applied horizontally one inch from the center of the beam to measure compressive strains (Figure 2a). The locations of the gauges are between the points of contact with the insulator to minimize damage to the gauges. The other two strain gauges used to measure tensile strains are applied horizontally one inch from the center of the beam between the two supports (Figure 2b). The face of the fastening system shoulder is ground away using a handheld grinder and straight edge to ensure the original dimensions, after placement of the LLED, are maintained.

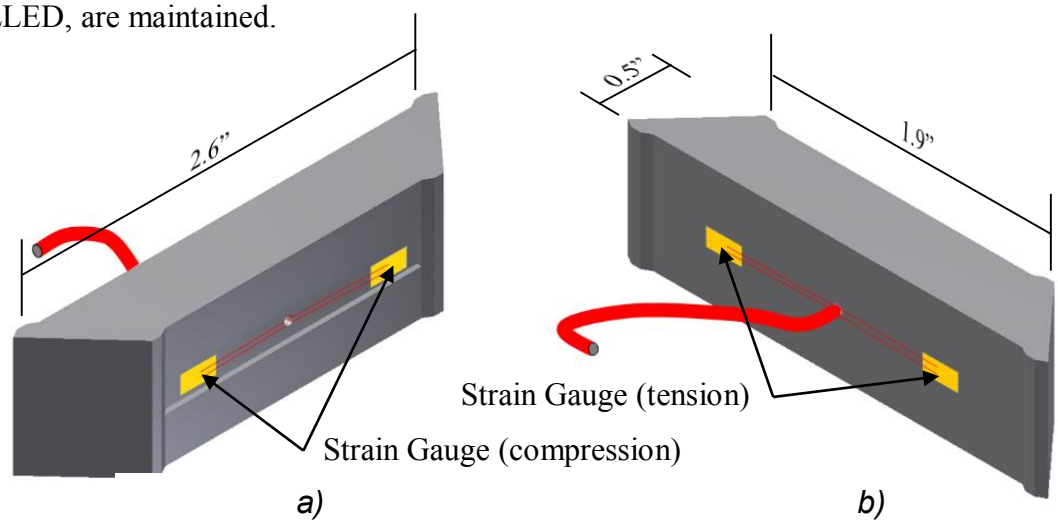

FIGURE 2 LLED strain gauge location and orientation.

Once the shoulder face is ground away, the LLED replaces it (Figure 3). The primary advantage of this technology is that the orignal fastening system geometry is maintained, thus clip installation procedures and all fastening system components remain the same. Furthermore,

material selection and geometry were also designed to reduce experimental error caused by different stiffnesses than an unaltered fastening system. Because lateral restraint is one of the fasteing system's primary functions, the LLED also will allow researchers to understand how variables associated with friction (e.g. materials and geometry) alter the lateral load path in addition to the magnitudes of lateral fastening system forces (*7*).

FIGURE 3 LLED installed in Safelok I fastening system.

LLED strain values are resolved into a force through calibration curves generated prior to testing using a uniaxial loading frame. LLEDs were supported on a level plate by two small steel blocks and loaded with a self-leveling loading head to ensure perpendicular loading during calibration. Loads were applied in 1,000 pound (1 kilopound (kip)) increments while corresponding strains were recorded. A thin steel insert is placed between the insulator and the two points of contact on the beam to ensure the points of loading would not penetrate into the comparatively soft insulator material (Nylon 6/6). If this did happen, it would turn the two-point load into a distributed load, negatively impacting the accuracy of the results (*6*). The stiffness of the beam and insert were chosen such that the stiffness of the system remained similar to its original condition. The result is a load cell at the shoulder-insulator interface that preserves the original geometry and ensures that the load path within the fastening system remains unaffected.

BACKGROUND

UIUC and other researchers have succeeded in measuring and quantifying the load path in the vertical direction through the use of strain gauges and additional instrumentation in the fastening system (*8*). Additionally, researchers at UIUC have successfully implemented matrix based tactile surface sensors (MBTSS) to measure the pressure distribution in the vertical direction at the interface of the rail pad and concrete rail seat (*9*). However, there have been few, if any, attempts to quantify and understand the mechanisms of lateral force restraint in the fastening system at a level that would guide design and maintenance practices (*10*). Furthermore, the mechanisms by which lateral forces are restrained (i.e. bearing or frictional forces) are not well understood.

For the Safelok I fastening system, it is assumed that the majority of the lateral forces from wheels are restrained by bearing forces (e.g. acting on the shoulder) and frictional forces

(e.g. acting between the rail and rail pad and the rail pad and rail seat). This relationship is expressed in Equation 1.

$$L_R = \Sigma L_B + \Sigma L_F \quad (1)$$

where,

L_R = Total lateral restraining force
ΣL_B = Summation of lateral bearing forces
ΣL_F = Summation of lateral frictional forces

All lateral bearing forces within a fastening system are measured by the LLED because there are no other surfaces for lateral forces to bear on in a Safelok I type fastening system. Lateral bearing restraint forces are affected by geometric tolerances within the track structure and fastening system as well as the lateral fastening system stiffness (*11*). Lateral frictional restraint forces occur at the interfaces between the rail and rail pad as well as the rail pad and rail seat. Lateral frictional restraint forces are affected by the vertical wheel load, fastening system component material properties, and their frictional characteristics relative to one another. Lateral frictional restraint forces are assumed to be the difference between the applied lateral wheel load and the sum of all consecutive LLEDs (i.e. lateral bearing forces). Frictional forces require a force normal to the plane of the interface between two surfaces, and the relationship is expressed in Equation 2.

$$L_F = \mu N \quad (2)$$

where,

L_F = Lateral frictional forces
μ = Coefficient of friction (COF) between rail pad and rail seat
N = Vertical wheel load (i.e. force applied normal to frictional planes)

This paper presents results from field experiments that were designed to understand the variables that affect the lateral force restraint mechanisms in the fastening system. To better understand the relationship between lateral bearing and frictional restraint forces, the following points are investigated:

- Effect of lateral frictional restraint forces (ΣL_F) on total lateral restraining force (L_R) by only varying applied vertical wheel load (i.e. force applied normal to frictional planes)
- Percentage of total lateral restraining force (L_R) that is restrained by lateral bearing or frictional forces (ΣL_B or ΣL_F) as applied lateral wheel load increases
- Lateral restraint forces under dynamic loading

EXPERIMENTAL FIELD SETUP

Figure 4 shows the location and naming convention of instrumentation within each test section. Field experiments and results described in this paper were conducted on a segment of tangent track on the Railroad Test Track (RTT) and a segment of curved track on the High Tonnage Loop (HTL) at the Transportation Technology Center (TTC) in Pueblo, Colorado. Different

static loading scenarios (e.g. load magnitudes, L/V ratios, etc.) were applied to the track using the Track Loading Vehicle (TLV) owned by the Association of American Railroads (AAR). The TLV uses a deployable axle capable of applying various combinations of vertical and lateral loads to simulate typical track loading conditions. A heavy axle load (HAL) freight train was used to measure the lateral response of the fastening system under dynamic and impact loading conditions on the HTL at speeds of 2, 15, 30, 40, and 45 mph. The HAL freight train consisted of three six-axle locomotives and ten freight cars of varying weights and was used to simulate the dynamic loading of a freight train. Both test sections consisted of a 136RE rail section, concrete crossties spaced at 24 inches center-to-center, Safelok I type fastening systems, and premium ballast. LLEDs were installed on the field side of the rail on both rail seats of three adjacent concrete crossties. Data were recorded at a sampling rate of 2,000 Hertz to maximize the number of samples taken during each static and dynamic test. All instrumentation was zeroed after installation and before any experimental data was recorded. Zeroing all instrumentation after installation and before experimental runs were conducted removed any successive forces or displacements associated with installation procedures, and produced data that quantified the applied static forces from the TLV or dynamic forces from passing trains.

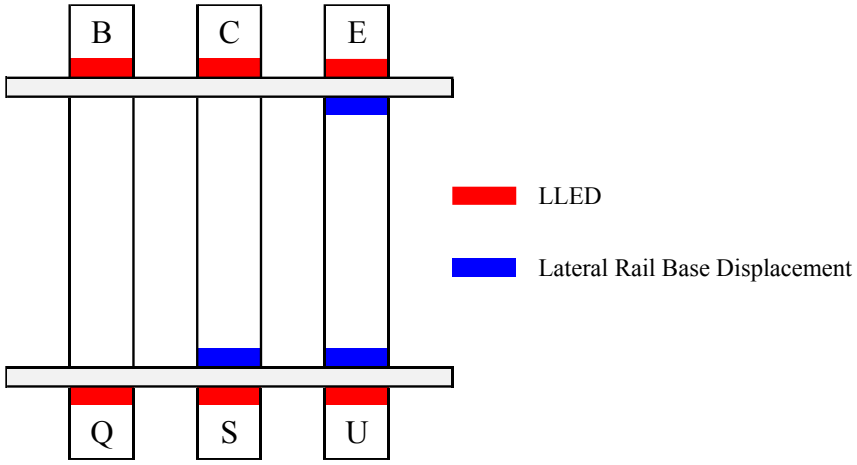

FIGURE 4 Instrumentation location and naming convention.

EFFECT OF VARYING APPLIED VERTICAL WHEEL LOAD

The RTT was chosen for static testing to minimize variability due to vehicle-track dynamics in the curve. The LLED at rail seat Q on the RTT was compromised during static testing, making any data gathered from the LLED unreliable. However, rail seats B, C, E, S, and U functioned properly (Figure 4). Data from the five functioning rail seats were analyzed to understand the influence of lateral wheel loads on lateral restraint forces in the fastening system. Figure 5 shows the average magnitude of lateral bearing restraint forces measured by the LLEDs for given lateral wheel loads under constant 20 kip and 40 kip vertical wheel loads applied by the TLV directly over the specified rail seat. Each data point represents five replicates and the error bars represent one standard deviation.

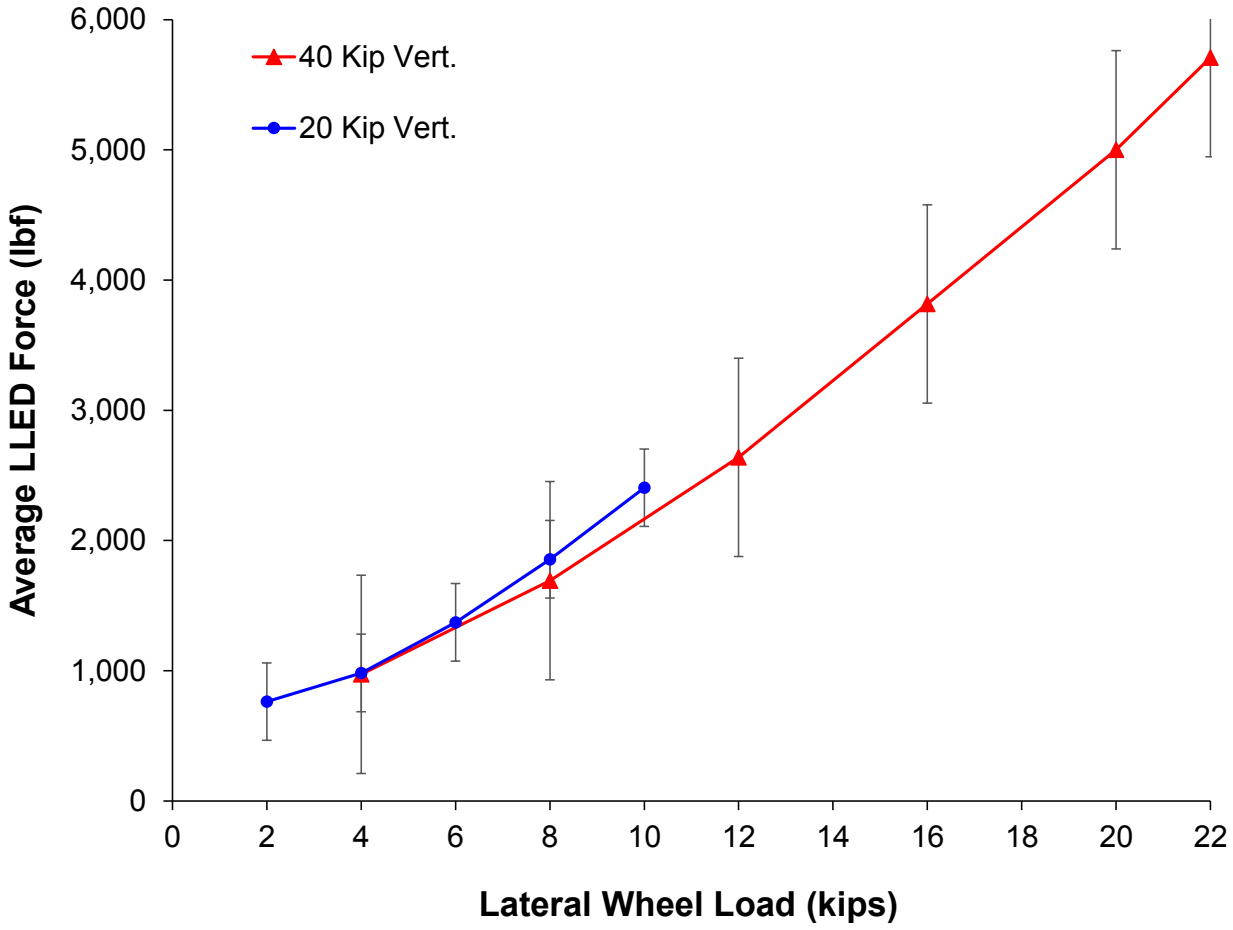

FIGURE 5 Average LLED force per rail seat as a function of lateral wheel load.

The trend of the curves for 20 kip and 40 kip applied vertical wheel loads are similar. As the applied lateral wheel load increases under a constant vertical wheel load, an upward trend of lateral bearing restraint forces (i.e. forces measured by the LLED) can be seen. This is likely due to the theoretically constant frictional force from the constant vertical wheel load under all lateral loading conditions. However, the rate at which the slope of the curve increases appears to be greater under a 20 kip applied vertical wheel load. At four kips of applied lateral wheel load, the LLED force is approximately 1,000 lbf for both vertical loading conditions. As the lateral wheel load increases to eight kips, the LLED forces increase to approximately 1,850 lbf and 1,700 lbf under a 20 kip and 40 kip vertical wheel load, respectively, a difference of 150 lbf. As the lateral wheel load increases to ten kips, the LLED forces increase to approximately 2,400 lbf under a 20 kip vertical wheel load and 2,150 lbf when interpolated under a 40 kip vertical wheel load, a difference of 250 lbf. The increase in the difference between LLED forces under equivalent lateral loads with varied vertical loads indicates that the lower magnitude of vertical wheel load may result in higher lateral bearing restraint forces due to the lower magnitude of force applied normal to the frictional planes. However, this increase in the difference between LLED forces under equivalent lateral loads with varied vertical loads is not in accordance with Equation 2. If the vertical wheel load doubles from 20 kips to 40 kips, the frictional forces should theoretically double, as well, causing the bearing forces at similar lateral loads to decrease.

A reasonable conclusion cannot be drawn from Figure 5 about the effect of vertical wheel loads on both the lateral bearing and frictional restraint forces. This behavior is further confirmed through Figure 6 which shows the sum of lateral forces from rail seats B, C, and E as a function of lateral wheel load under constant 20 kip and 40 kip vertical wheel loads applied by the TLV. Based on Equation 1 and Equation 2, the difference between the lines for total frictional and bearing forces under a 20 kip vertical load should be smaller than under a 40 kip vertical wheel load (i.e. bearing forces should increase and frictional forces should decrease). However, both 20 kip and 40 kip vertical wheel load plots appear to produce similar results for both frictional and bearing force. Because these circumstances do not agree with the theoretical equations, this is an area for future research.

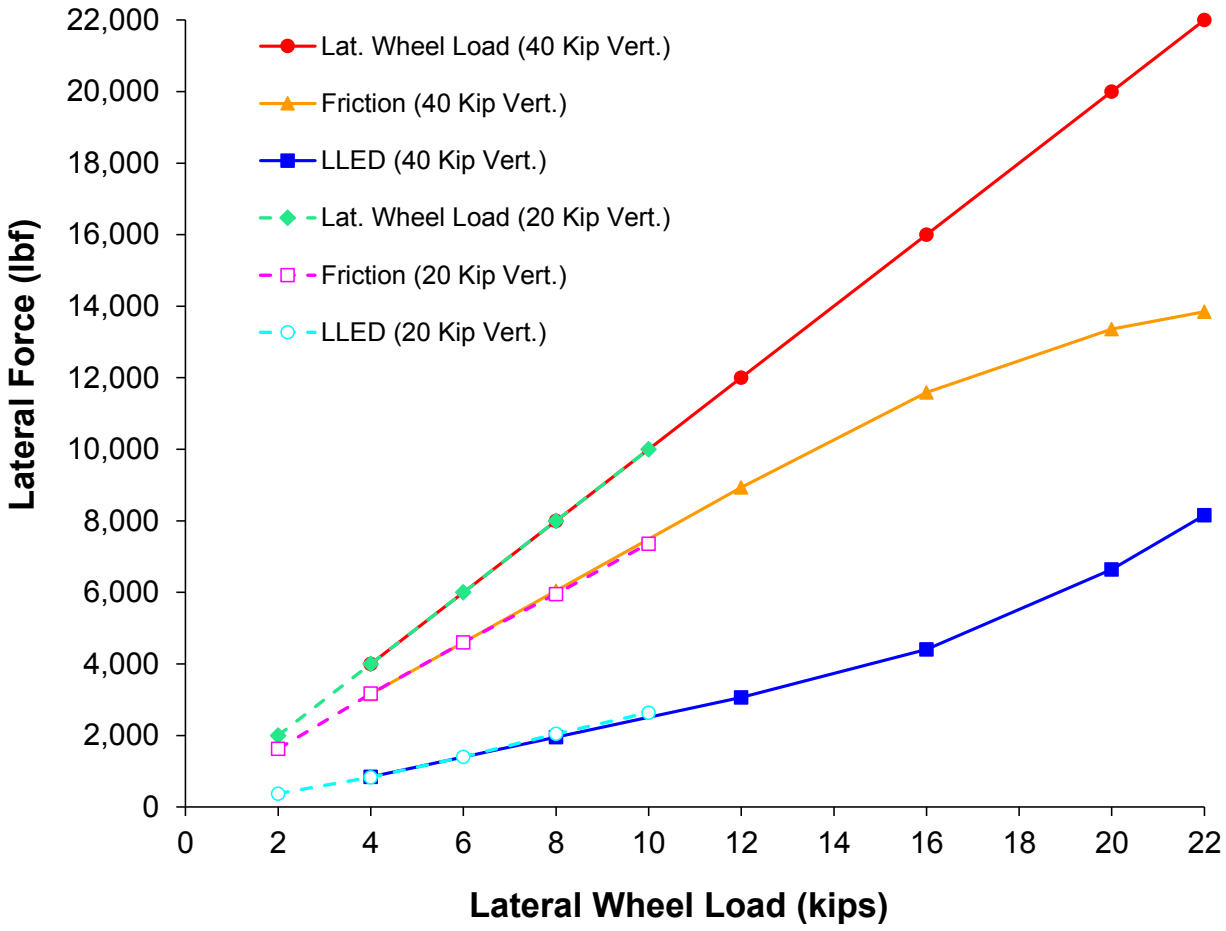

FIGURE 6 Sum of lateral fastening system forces on rail seats B, C, and E as a function of lateral wheel load.

PERCENTAGE OF LATERAL RESTRAINT FORCES

As previously mentioned, lateral frictional restraint forces are assumed to be the difference between the applied lateral wheel load and the sum of all consecutive LLEDs (i.e. lateral bearing restraint forces). As the applied lateral wheel load increases, the lateral frictional and bearing restraint forces begin to converge (Figure 6). A similar converging trend has also been observed through the analysis of results from UIUC's 3-D finite element (FE) model of the same crosstie and fastening system used in the field (*12*). The similar results from both field experimentation

and FE model data show the converging trend is what occurs within the fastening system as lateral wheel load increases. The trend indicates that the percentage of applied lateral wheel load restrained by frictional forces decreases while the percentage of applied lateral wheel load restrained by bearing forces increases, imparting a higher load on the insulator.

Figure 7 shows the change in lateral restraint forces as a function of lateral wheel load in two ways: the ratio of frictional forces to bearing forces and lateral bearing restraint forces as a percentage. As the applied lateral wheel load increases, the ratio of frictional forces to bearing forces decreases from approximately 3.7 at 4 kips of lateral wheel load to 1.7 at 22 kips of lateral wheel load, a decrease of 54%. The percentage of the applied lateral wheel load restrained by lateral bearing restraint forces increases from approximately 21% at four kips of lateral wheel load to 37% at 22 kips of lateral wheel load, an increase of 16%. This indicates that as the lateral wheel load increases, the demands on the insulator and shoulder increase due to more of the lateral wheel load being restrained by bearing forces.

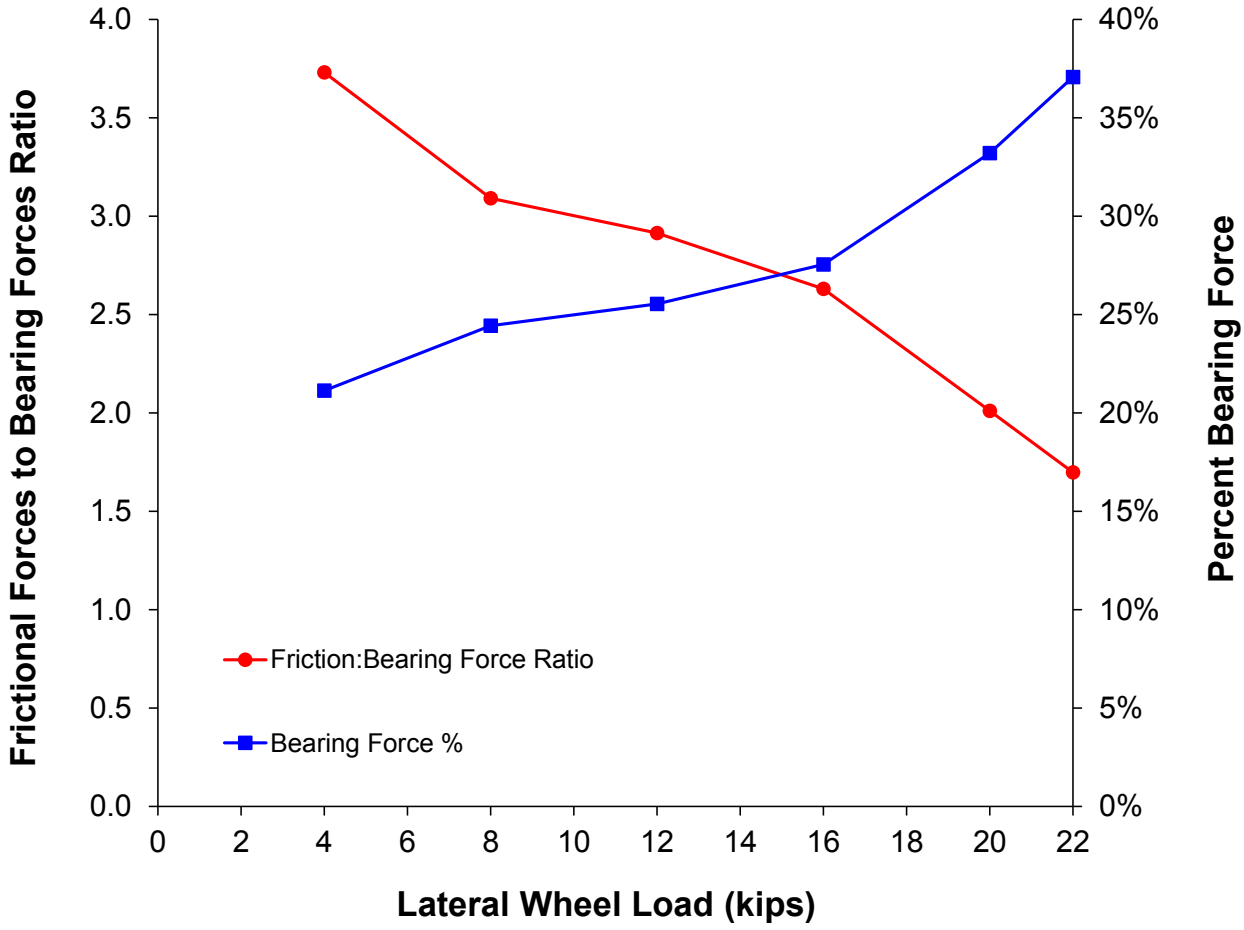

FIGURE 7 Change in lateral restraint forces as a function of lateral wheel load.

STATIC VERSUS DYNAMIC LATERAL RESTRAINT FORCES

Figure 8 shows peak LLED forces under a HAL freight train from all axles and tested speeds as a function of lateral wheel load. The data indicate that at 20 kips of lateral wheel load, the lateral bearing restraint force will be approximately 7,000 lbf for rail seat U and 10,700 lbf when extrapolated for rail seat E. This would equate to a percentage of applied lateral wheel load

restrained by lateral bearing forces of 35% and 54% for rail seats U and E, respectively. Although the data cannot be directly compared due to different testing locations (RTT vs. HTL), it can be noted that rail seat U on the low rail of the HTL behaved similarly to the averaged data from the RTT. However, rail seat E on the high rail of the HTL produced much higher magnitudes of lateral bearing forces than the remaining data. Such a high percentage of lateral bearing forces under dynamic loads may be due to the rate of load application from the passing train and its effect on the frictional characteristics of the system, as well as the track geometry.

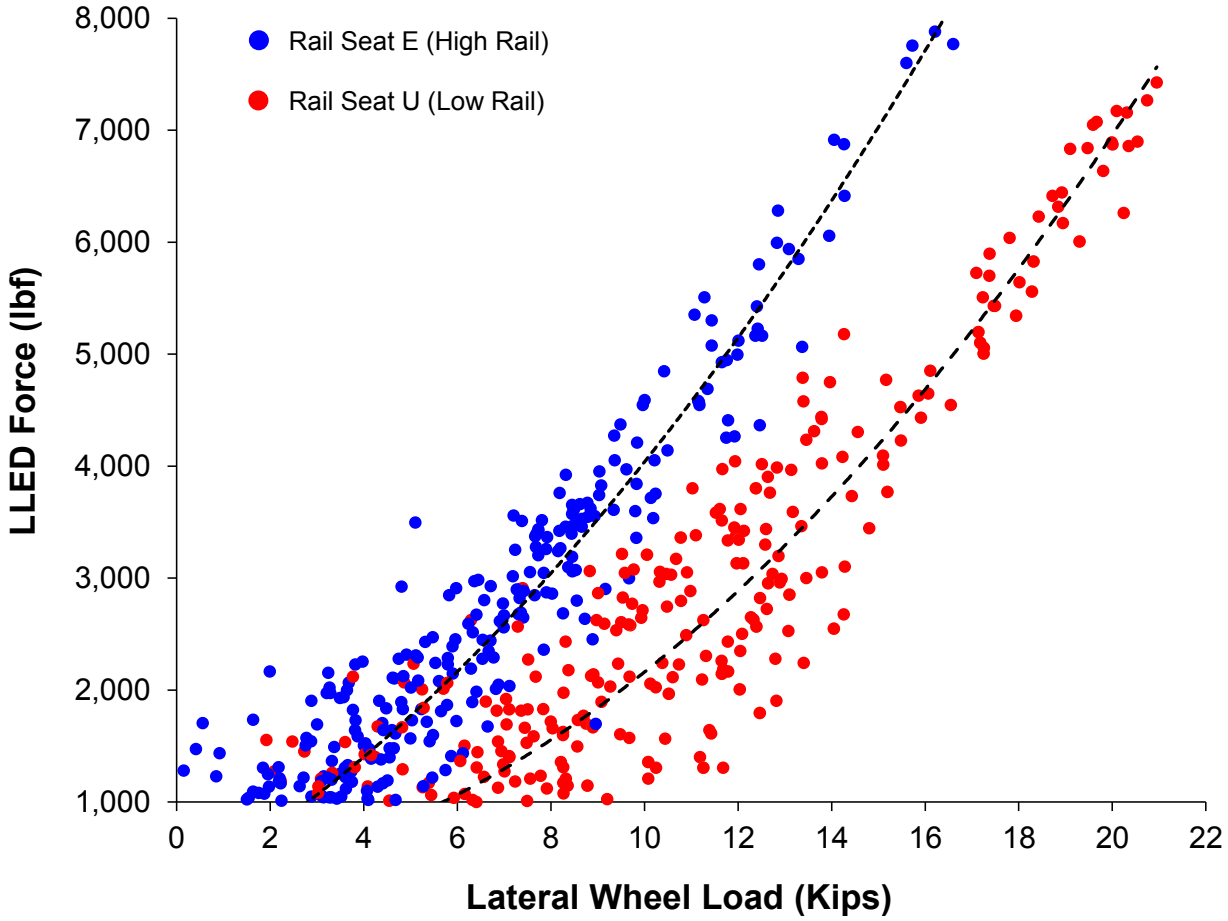

FIGURE 8 Peak LLED forces under HAL freight train as a function of lateral wheel load.

Although there appears to be a correlation between lateral bearing forces and lateral wheel loads, there is still a large amount of variability between the two metrics. Previous work has been conducted to understand the role friction plays on abrasion mechanisms of the concrete rail seat, as well as the role lateral fastening system stiffness plays on the magnitudes of lateral bearing forces (*11, 13*). Despite this work, a comprehensive understanding of the role friction plays in the transfer of lateral wheel loads into the fastening system does not exist (*11, 13*). This work will be continued with a stronger emphasis on the frictional characteristics of the fastening system and its effect on lateral restraint forces in concrete crosstie fastening systems.

CONCLUSIONS

Lateral Load Evaluation Devices (LLEDs) developed at UIUC have proven to be a successful tool to quantify lateral restraint forces on the shoulder. Two governing equations, Equation 1: $L_R = \Sigma L_B + \Sigma L_F$, and Equation 2: $L_F = \mu N$ guided this research to better understand how lateral forces are restrained. Static and dynamic observations from the field show a high degree of correlation and result in the following preliminary conclusions and observations:

- Under equivalent lateral loading conditions, lower magnitudes of vertical wheel load (i.e. force applied normal to frictional planes) may result in higher lateral bearing restraint forces due to the lower magnitude of force applied normal to the frictional planes. However, the difference between constant 20 kip and 40 kip applied vertical wheel load with increasing lateral wheel load is smaller than hypothesized.

- As lateral wheel load increases, the lateral frictional and bearing restraint forces begin to converge. This indicates that the percentage of the applied lateral wheel load restrained by frictional forces (ΣL_F from Equation 1) starts to decrease while the percentage of the applied lateral wheel load restrained by bearing forces (ΣL_B from Equation 1) starts to increase.

- As static lateral wheel load increases, the ratio of frictional forces to bearing forces decreases from approximately 3.7 at 4 kips of lateral wheel load to 1.7 at 22 kips of lateral wheel load, a decrease of 54%. The percentage of the applied lateral wheel load restrained by lateral bearing restraint forces increases from approximately 21% at four kips of lateral wheel load to 37% at 22 kips of lateral wheel load, an increase of 16%.

- In the dynamic lateral loading case, there is increased variability in the lateral loads restrained by bearing forces resulting in increased demands on the fastening system components. For example, the percentage of applied lateral wheel load restrained by lateral bearing forces for rail seats U and E were 35% and 54%, respectively. Though rail seat U exhibits behavior similar to the static results, the bearing force measured from rail seat E exceeds the results from the static analysis by 17%.

In addition to further investigating the role of friction in the performance of the fastening system through controlled laboratory experimentation, future work will include separating the data by rolling stock type (i.e. locomotives, loaded freight cars, empty freight cars, and passenger cars) to investigate the effects of varying train type and their mechanical characteristics. This could provide railroads and suppliers with valuable insight into the demands that mixed traffic impart on the track.

Future fastening system designs will benefit from the presented results by incorporating the data into a mechanistic design approach by designing systems with optimum lateral load transfer characteristics such as material selection and frictional properties. The results from these LLED experiments will also be beneficial in validation of finite element modeling (FEM) work also being conducted at UIUC. Moreover, the results will be used to aid in future fastening system designs to mitigate current recurring problems seen on North American heavy-haul freight railroads.

ACKNOWLEDGEMENTS

This project is sponsored by a grant from the Association of American Railroads (AAR) Technology Outreach Program with additional funding for field experimentation provided by the United States Department of Transportation (DOT) Federal Railroad Administration (FRA). The published material in this paper represents the position of the authors and not necessarily that of DOT. The authors would like to thank David Davis of AAR/TTCI and the members of the AAR Technology Outreach Committee; John Bosshart and Thomas Brueske of BNSF; Harold Harrison of H2 Visions, Inc.; Don Rhodes and Bill Rhodes of Instrumentation Services, Inc.; Tim Prunkard, Darold Marrow, and Don Marrow of the University of Illinois at Urbana-Champaign (UIUC); Jose Mediavilla of Amsted RPS; Jim Beyerl of CSX Transportation; Steve Ashmore and Chris Rewczuk of UPRR; and Bob Coats of Pandrol USA for their advice, guidance and contributions to this research. The authors would also like to acknowledge Daniel Kuchma, David Lange, Thiago Bizarria, Christopher Rapp, Brandon Van Dyk, Sihang Wei, Justin Grasse, Kartik Manda, and Andrew Scheppe from UIUC for their work on this research. J. Riley Edwards has been supported in part by the grants to the UIUC Railroad Engineering Program from CN, Hanson Professional Services, and the George Krambles Transportation Scholarship Fund.

REFERENCES

1. Van Dyk, B. et al 2012. *International Concrete Crosstie and Fastening System Survey – Final Results*, University of Illinois at Urbana-Champaign, Results Released June 2012.
2. Hay, W.W. *Railroad Engineering*, *2nd ed.*, John Wiley & Sons, Inc., New York City, New York, 1982, Ch. 23, pp. 471-473.
3. *AREMA Manual for Railway Engineering*, American Railway Engineering and Maintenance-of-Way Association (AREMA), Landover, Maryland, 2012, v 1, ch. 30, parts1 and 4.
4. Stamatis, D, H. *Failure Mode and Effect Anaylsis: FMEA From Theory to Execution*.Vol.1. Milwaukee: ASQC Quality Press, 1995. 1-482. Print.
5. Painter, P.C and M.M. Coleman. *Essentials of Polymer Science and Engineering,* DEStech Publications, Inc., Lancaster, PA.
6. Van Dyk, B., J. R. Edwards, C.J. Ruppert, and C.P.L Barkan. 2013. Considerations for Mechanistic Design of Concrete Sleepers and Elastic Fastening Systems in North America. In: *Proceedings: International Heavy Haul Association Conference*, New Delhi, India, February 2013.
7. Czichos, H. 1978. *Tribology: a systems approach to the science and technology of friction, lubrication and wear*, Elsevier North-Holland, Inc., New York, NY.
8. Grasse, J. 2013. *Field Test Program of the Concrete Crosstie and Fastening System.* University of Illinois at Urbana-Champaign, Urbana, IL.
9. Rapp, C.T., M. Dersch, J.R. Edwards, C.P.L. Barkan, B. Wilson, and J. Mediavilla. 2013. Measuring Concrete Crosstie Rail Seat Pressure Distribution with Matrix Based Tactile Surface Sensors. In: *Proceedings: Transportation Research Board Annual Meeting,* Washington D.C., United States, January 2013, pp. 2-3
10. Rhodes, Don, Instrumentation Services, Inc. Personal interview, 19 March 2013.,
11. Williams, B., R. Kernes, J. R. Edwards, and C. P. L. Barkan. 2014. Lateral Force Measurement in Concrete Crosstie Fastening Systems. In: *Proceedings: Transportation Research Board Annual Meeting,* Washington D.C., United States, January 2014, pp. 8-10.
12. Chen, G. C., M. Shin, B. Andrawes. (2013). Finite Element Modeling of the Fastening Systems and the Concrete Sleepers in North America. [PowerPoint slides]. New Delhi: International Heavy Haul Association. Available at: Rail Transportation and Engineering Center. <http://moodle.bcu.ac.uk/health/course/view.php?id=1356> (accessed 1 March 2013).
13. Kernes, R., J. R. Edwards, D. Lange, and C. P. L. Barkan. 2011. Investigation of the Dynamic Frictional Properties of a Concrete Crosstie Rail Seat and Pad and its Effect on Rail Seat Deterioration (RSD). In: *Proceedings: Transportation Research Board Annual Meeting,* Washington D.C., United States, January 2011, pp. 6-10.